Shape Preserving Surface Reconstruction Using Locally Anisotropic Radial Basis Function Interpolants

G. Casciola, D. Lazzaro, L. B. Montefusco and S. Morigi
Department of Mathematics, University of Bologna
P.zza di Porta San Donato 5, 40127 Bologna, Italy
casciola@dm.unibo.it   lazzaro@csr.unibo.it   <montelau><morigi>@dm.unibo.it

Abstract—In this paper we deal with the problem of reconstructing surfaces from unorganized sets of points, while capturing the significant geometry details of the modelled surface, such as edges, flat regions, and corners. This is obtained by exploiting the good approximation capabilities of the radial basis functions (RBF), the local nature of the method proposed in [1], and introducing information on shape features and data anisotropies detected from the given surface points.

The result is a shape-preserving reconstruction, given by a weighted combination of locally anisotropic interpolants. For each local interpolant the anisotropy is obtained by replacing the Euclidean norm with a suitable metric which takes into account the local distribution of the points. Thus hyperellipsoid basis functions, named anisotropic RBFs, are defined. Results from the application of the method to the reconstruction of object surfaces in $\mathbb{R}^3$ are presented, confirming the effectiveness of the approach. © 2006 Elsevier Ltd. All rights reserved.

Keywords—Radial basis function, Shape preserving, Surface reconstruction, Local interpolation.

1. INTRODUCTION

Surface reconstruction is concerned with the generation of continuous models from unorganized sets of points. This problem arises in a wide range of scientific and engineering applications, as well as in computer graphics and computer vision where these points come from the digitalization of model surfaces. Creating accurate models of real objects from digital scans or surface sketching is currently the subject of intensive research. In these cases, in order to obtain high quality surface reconstructions, it is very important to recover the surface shape, especially for objects with sharp features (edges, corners, spikes, etc.).

In this paper, we will focus on the reconstruction of implicit surfaces that accurately capture and reproduce the shape of the data. The implicit representation is based on a local use of radial basis functions (RBFs) and we propose an anisotropic extension of these functions to allow the surface to locally follow the geometry of the data.

More precisely, the reconstruction problem we consider here can be posed as follows.

Let Ω be a compact set and let the distinct point sets $X_0 = \{\mathbf{x}_i\}_{i=1}^{N_0}$ and $X_1 = \{\mathbf{x}_i\}_{i=N_0+1}^{N} \subset \Omega \subset \mathbb{R}^3$ be given. The set X_0 represents the digitalisation of an object surface, that is, the points $\mathbf{x}_i$ are on the unknown surface, while the off-surface point set X_1 is simply a mathematical instrument allowing us to use an implicit approach to the reconstruction problem. Both sets can be provided, e.g., by a 3D laser scanner, if the line-of-sight to the scanner is used during the acquisition phase. We associate with the data set $X = X_0 \bigcup X_1$ a set $\Im \in \mathbb{R}$ of corresponding values of a *signed-distance function*, namely, $f_i = 0$, $i = 1, \ldots, N_0$ and $f_i = d_i \neq 0$, $i = N_0 + 1, \ldots, N$, where $d_i > 0$ for points outside the object surface and $d_i < 0$ for points inside.

The *implicit shape-preserving reconstruction* problem consists of determining a function $F(\mathbf{x})$ which implicitly models the unknown surface by satisfying the interpolation conditions

$$F(\mathbf{x}_i) = 0, \qquad i = 1, \ldots, N_0 \qquad \text{(on-surface constraints)}, \tag{1}$$

$$F(\mathbf{x}_i) = d_i, \qquad i = N_0 + 1, \ldots, N \quad \text{(off-surface constraints)}, \tag{2}$$

and which has the property that its zero-set $F_0 = \{\mathbf{x} \in \mathbb{R}^3; \ F(\mathbf{x}) = 0\}$ *preserves the local behaviour of the surface points.*

This distance function $F(\mathbf{x})$ gives us an implicit, but analytical representation of the object surface, allowing it to be evaluated anywhere to produce a mesh at the desired resolution, thus offering a meshfree 3D reconstruction.

In this paper, we consider radial basis functions for the implicit representation of object surfaces, since these functions represent a well-established tool for multivariate scattered data interpolation. Several works exist in the literature devoted to the reconstruction of surfaces using RBFs starting from unorganized point sets (see, e.g., [2-5]). However, most of these works calculate the implicit surface globally, by solving a large and sometimes dense linear system, with consequent limitations of the number of points that can be processed and with related problems regarding stability and computational cost. Another lack in the global reconstruction with RBFs seems to be the difficulty to globally model the different local behaviors of the surface points near object shape features. The implicit function, in fact, should fit the data, so that the shape of its zero-set follows at best the local geometry of the object surface, that is, it accurately captures structured features such as corners, edges, and flat regions. To obtain this result, it would be necessary to scale the radial basis functions differently, according to the local data density, or to distort the shape of some basis functions to capture local anisotropies, which identify particular features, in the data. Unfortunately, adapting the basis functions is, in general, not allowed in the global case, as the solvability of the interpolation problem is no longer guaranteed. Even if this problem has been considered in [6], and sufficient conditions are given for its unique solvability, it seems rather difficult to apply these conditions in practice.

To overcome the limitations imposed by a global approach, in [1], a local RBF interpolation method has been proposed, which allows for efficiently dealing with very large data sets.

The main idea of this local method is to divide the global domain Ω into smaller overlapping domains $\{\Omega_j\}_{j=1,\ldots,N}$ where the RBF interpolation problem can be solved locally. Associated with this covering, a family of nonnegative weight functions $\{w_j\}_{j=1,N}$, with limited support $\text{supp}(w_j) \subseteq \Omega_j$, is constructed, with the additional property that $\sum_j w_j = 1$ in the entire domain Ω. The local solutions are finally blended together, using these weighting coefficients to obtain a smooth, locally defined global interpolant.

In [7], the performance of this local RBF interpolation method has been tested for the reconstruction of large data sets and an efficient hole-filling procedure has also been proposed, exploiting the local nature of the method.

In this paper we consider a generalization of the proposal in [1] in order to deal with local anisotropy in the data. The basic idea is to consider small homogeneous subsets of data on which to evaluate the local interpolants, and, for each of them, to replace the Euclidean metric by a suitable metric in $\mathbb{R}^d$, which allows the RBF to be distorted into functions with hyperellipsoids

as level sets. In this way the problems arising in the global approach are avoided, since the same metric is considered for all RBFs used in each local interpolation. The corresponding linear system is thus uniquely solvable. Moreover, in order to follow the anisotropy of the data, all the weight functions are also distorted, according to the same metric, but without destroying their original properties.

An important step in this new approach is to choose the metric in order to model the local data anisotropy. Following a popular signal processing method for feature extraction, we perform, for each local data set, the principal component analysis of the covariance matrix, in order to determine the direction of the data anisotropy. Then the most natural choice is to use the inverse of the covariance matrix to define the appropriate metric. The effectiveness of this choice is confirmed by several experimental results.

The rest of the paper is organized as follows. In Section 2 we present some theoretical results on anisotropic interpolation with RBFs in $\mathbb{R}^d$. In Section 3 we introduce anisotropic interpolation in the local method presented in [1] and the properties of the modified weight functions are proved. In Section 4, we restrict ourselves to the case of surface reconstruction in $\mathbb{R}^3$: we first give an overview of the method we used to classify the local features of surface points, then we present results of the application of this detected information both to suitably scale the RBFs, and to deal with anisotropic RBFs in the local interpolation processes.

2. ANISOTROPIC INTERPOLATION WITH RADIAL BASIS FUNCTIONS

Let Ω be a compact set, $X = \{\mathbf{x}_i\}_{i=1}^N \subset \Omega \subset \mathbb{R}^d$ be a set of distinct nodes, and $\Im = \{f_i\}_{i=1}^N \subset \mathbb{R}$ be a set of function values. Let us denote by $\mathbb{P}_m^d$ the space of d-variate polynomials of order not exceeding m. The RBF interpolant of the data

$$\{(\mathbf{x}_i, f_i)\}_{i=1}^N, \qquad \mathbf{x}_i \in X, \quad f_i \in \Im, \tag{3}$$

with conditionally positive definite radial function $\varphi : \mathbb{R}_{\geq 0} \to \mathbb{R}$ of order $m \geq 0$ is given by

$$R(\mathbf{x}) = \sum_{j=1}^N a_j \varphi(\|\mathbf{x} - \mathbf{x}_j\|_2) + \sum_{i=1}^n b_i p_i(\mathbf{x}), \tag{4}$$

where $n = \dim \mathbb{P}_m^d$, and $\{p_i\}_{i=1,\dots,n}$ is a basis for $\mathbb{P}_m^d$. The coefficients a_j, $j = 1, \dots, N$, and b_i, $i = 1, \dots, n$, are obtained from the conditions $R(\mathbf{x}_i) = f_i$, $i = 1, \dots, N$, i.e., by solving the linear system

$$\begin{aligned} A\mathbf{a} + P\mathbf{b} &= \mathbf{f}, \\ P^\top \mathbf{a} + 0 &= \mathbf{0}, \end{aligned} \tag{5}$$

with

$$\begin{aligned} A &= (\varphi(\|\mathbf{x}_i - \mathbf{x}_j\|_2))_{i,j=1,\dots,N}, \\ P &= (p_j(\mathbf{x}_i))_{i=1,\dots,N, \, j=1,\dots,n}. \end{aligned}$$

It is well known that system (5) is uniquely solvable, as long as the following additional assumption holds:

$$\text{rank}(P) = n \leq N. \tag{6}$$

Let M now be a $d \times d$ nonsingular real matrix and $Y \subset \mathbb{R}^d$ the set $Y = \{\mathbf{y}_i; \mathbf{y}_i = M\mathbf{x}_i, \mathbf{x}_i \in X\}$. If we consider the RBF interpolation problem on the transformed data

$$\{(\mathbf{y}_i, f_i)\}_{i=1}^N, \qquad \mathbf{y}_i \in Y, \quad f_i \in \Im, \tag{7}$$

it is straightforward to see that it is still uniquely solvable, since the nonsingular matrix M represents an affine transformation, and the new set Y satisfies relation (6), too.

This new RBF interpolant takes the form

$$R(\mathbf{y}) = \sum_{j=1}^{N} \alpha_j \varphi(\|\mathbf{y} - \mathbf{y}_j\|_2) + \sum_{i=1}^{n} \beta_i p_i(\mathbf{y})$$

and can be characterized as follows.

THEOREM 1. *Let* $\{(\mathbf{x}_i, f_i)\}_{i=1}^{N}$, $\mathbf{x}_i \in X \subset \Omega \subset \mathbb{R}^d$, $f_i \in \Im \subset \mathbb{R}$ *be a data set for which the linear system (5) is uniquely solvable. Let M be a nonsingular $d \times d$ matrix that maps the sets X and Ω into the sets Y and $\bar{\Omega}$, respectively. Then*

$$R(\mathbf{y}) = R_T(\mathbf{x}),$$

where

$$R_T(\mathbf{x}) = \sum_{j=1}^{N} \alpha_j \varphi(\|\mathbf{x} - \mathbf{x}_j\|_T) + \sum_{i=1}^{n} \beta_i p_i(\mathbf{x}) \tag{8}$$

is the "anisotropic" RBF interpolant on the original data, and $T = M^\top M$.

PROOF. Since M is nonsingular, the matrix T is a positive definite matrix. Thus the function $\|\cdot\|_T : \mathbb{R}^d \to \mathbb{R}_{\geq 0}$, defined as

$$\|\mathbf{x}\|_T = \sqrt{\mathbf{x}^\top T \mathbf{x}} = \sqrt{\mathbf{x}^\top M^\top M \mathbf{x}} = \|M\mathbf{x}\|_2,$$

is a norm of $\mathbb{R}^d$. Now, recalling that the space $\mathbb{P}_m^d$ of multivariate polynomials is affine invariant, the result follows immediately.   ∎

The previous result shows that the RBF interpolant on the transformed data can be seen as a metric adjusted RBF interpolant on the original data. This observation justifies the following definition.

DEFINITION 1. *Let* $\Phi_j(\cdot) = \varphi(\|\cdot - \mathbf{x}_j\|_2)$ *be a radial basis function with center $\mathbf{x}_j$, and let T be a symmetric positive definite matrix. We define anisotropic radial basis function as*

$$\Phi_{T,j}(\cdot) = \varphi(\|\cdot - \mathbf{x}_j\|_T),$$

namely a function whose level sets are hyperellipsoids, centered in $\mathbf{x}_j$, and associated with the quadratic form $(\mathbf{x} - \mathbf{x}_j)^\top T (\mathbf{x} - \mathbf{x}_j)$.

The anisotropic RBF interpolant $R_T(\mathbf{x})$ does not, in general, coincide with its isotropic version $R(\mathbf{x})$, unless the matrix T is the identity matrix. In fact, as pointed out in [8], RBF interpolants are not affine invariant. Therefore it is necessary to study the aspects of stability and accuracy of approximation of this anisotropic interpolant. The critical quantities that need to be considered are the separation distance q_Y and the fill distance h_Y of the new set Y, which are defined by

$$q_Y = \frac{1}{2} \min_{1 \leq i < j \leq N} \|\mathbf{y}_i - \mathbf{y}_j\|_2, \qquad h_Y = \sup_{\mathbf{y} \in \bar{\Omega}} \min_{1 \leq i \leq N} \|\mathbf{y} - \mathbf{y}_i\|_2.$$

Their value characterizes the density of the set Y, and is therefore strongly dependent on the transformation matrix M. In particular, the following theorem gives the relation between these quantities and the separation and fill distances of the original set X.

THEOREM 2. *Let M be a $d \times d$ nonsingular matrix that maps the sets X and Ω into the sets Y and $\bar{\Omega}$, respectively, and let $T = M^{\top}M$ be the associated symmetric, positive definite matrix, whose eigenvalues are λ_i, $i = 1, \ldots, d$. The separation and fill distances of the sets X and Y satisfy*

$$\sqrt{\lambda_{\min}}q_X \le q_Y \le \sqrt{\lambda_{\max}}q_X, \tag{9}$$

$$\sqrt{\lambda_{\min}}h_X \le h_Y \le \sqrt{\lambda_{\max}}h_X. \tag{10}$$

PROOF. Set $\mathbf{d}_{ij} = \mathbf{x}_i - \mathbf{x}_j$ and $\boldsymbol{\delta}_{ij} = \mathbf{y}_i - \mathbf{y}_j$. We have that $\boldsymbol{\delta}_{ij} = M\mathbf{d}_{ij}$. Since

$$\frac{\|\boldsymbol{\delta}_{ij}\|_2^2}{\|\mathbf{d}_{ij}\|_2^2} = \frac{\mathbf{d}_{ij}^{\top}T\,\mathbf{d}_{ij}}{\mathbf{d}_{ij}^{\top}\mathbf{d}_{ij}},$$

by using the Rayleigh quotient properties, it follows

$$\lambda_{\min} \le \frac{\mathbf{d}_{ij}^{\top}T\,\mathbf{d}_{ij}}{\mathbf{d}_{ij}^{\top}\mathbf{d}_{ij}} \le \lambda_{\max},$$

that is,

$$\sqrt{\lambda_{\min}}\|\mathbf{x}_i - \mathbf{x}_j\|_2 \le \|\mathbf{y}_i - \mathbf{y}_j\|_2 \le \sqrt{\lambda_{\max}}\|\mathbf{x}_i - \mathbf{x}_j\|_2.$$

Relation (9) now follows, taking the minimum over i and j.

Analogously, for each $\mathbf{x} \in \Omega$ and $\mathbf{y} = M\mathbf{x} \in \bar{\Omega}$ we have

$$\sqrt{\lambda_{\min}}\|\mathbf{x} - \mathbf{x}_i\|_2 \le \|\mathbf{y} - \mathbf{y}_i\|_2 \le \sqrt{\lambda_{\max}}\|\mathbf{x} - \mathbf{x}_i\|_2,$$

thus setting

$$r(\mathbf{x}) = \min_i \|\mathbf{x} - \mathbf{x}_i\|_2 \qquad \text{and} \qquad r(\mathbf{y}) = \min_i \|\mathbf{y} - \mathbf{y}_i\|_2$$

and taking the minimum over i, we obtain

$$\sqrt{\lambda_{\min}}r(\mathbf{x}) \le r(\mathbf{y}) \le \sqrt{\lambda_{\max}}r(\mathbf{x}).$$

Letting $\mathbf{y}$ now vary over $\bar{\Omega}$, and correspondingly $\mathbf{x}$ over Ω, and taking the sup, we obtain (10). ∎
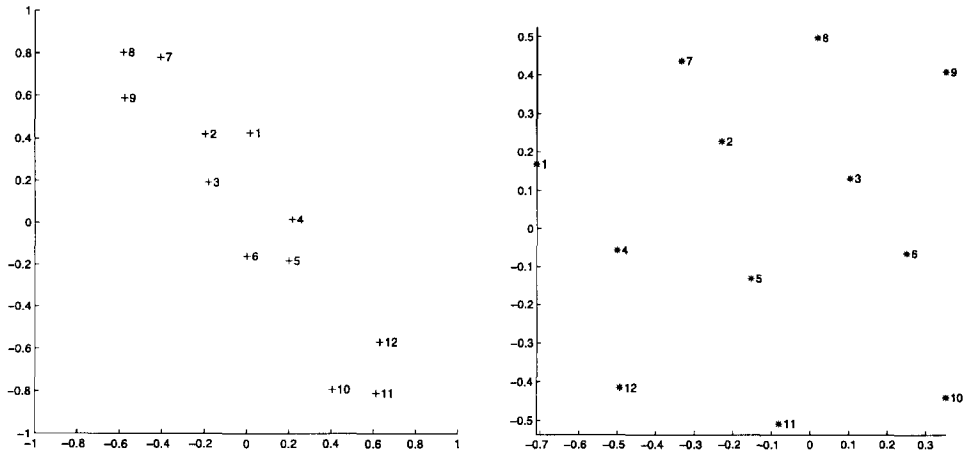

Figure 1. Nonuniform data set X (left) with $q_X = 0.088$, $h_X \approx 0.328$; transformed data set Y (right), obtained using $M = [-2.22, -1.59; -0.29, 0.41]$ with $q_Y = 0.117$, $h_Y \approx 0.272$.

The previous analysis shows that a "good" choice of the affine transformation represented by M can significantly improve the behaviour of the anisotropic RBF interpolant, concerning stability and accuracy of approximation according to the analysis given in [9–11]. In Section 4 we propose a possible choice for a transformation M, which produces very satisfactory results. In Figure 1, we show a simple 2D example, where a set X of severely nonuniform data is transformed into a quasi-uniform set Y, by choosing the transformation M, according to the criterion given in Section 4. The transformed set Y presents an increased separation distance q_Y, with consequent reduction of the condition number of the RBF matrix

$$A = (\varphi(\|\mathbf{y}_i - \mathbf{y}_j\|_2))_{i,j=1,\dots,N},$$

and a reduced fill distance h_Y, that gives a better reproduction quality of the anisotropic RBF interpolant.

3. LOCALLY ANISOTROPIC INTERPOLATION

In this section we introduce the concept of anisotropic radial basis functions in the reconstruction method presented in [1] and [7]. Since that method uses a weighted combination of local interpolants, based on inverse distance weights, we introduce a new metric, not only in the RBF interpolants, but also in the weight functions. This local strategy allows us to adapt the metric to the different data anisotropies, without needing to satisfy the strong conditions given in [6], where a global approach is considered.

Let the compact set Ω, the set of distinct nodes $X = \{\mathbf{x}_i\}_{i=1}^N \subset \Omega \subset \mathbb{R}^d$, and the set of the corresponding function values $\Im = \{f_i\}_{i=1}^N \subset \mathbb{R}$ be given. For each $\mathbf{x}_k \in X$, $k = 1, \dots, N$, we associate a symmetric positive definite matrix $T_k = M_k^\top M_k$ and a set $X_{T_k} = \{\mathbf{x}_i \in X, i \in I_k\}$, where I_k is the set of indexes of $N_q - 1$ *suitable* T_k-neighbours of $\mathbf{x}_k$, as well as $\mathbf{x}_k$ itself. The term T_k-neighbours denotes that the distance is measured using the norm induced by T_k and *suitable* means that T_k is chosen so that the corresponding elements of the set $Y_k = \{\mathbf{y}_i;\ \mathbf{y}_i = M_k\mathbf{x}_i,\ \mathbf{x}_i \in X_{T_k}\}$ satisfy certain conditions of uniform data density (see [7] and the references therein for details). Then we compute the nodal anisotropic RBF interpolant (8) on the set X_{T_k}, namely satisfying

$$R_{T_k}(\mathbf{x}_i) = f_i, \qquad i \in I_k.$$

Moreover, for each $\mathbf{x}_k$, we identify a hyperellipsoidal region of influence Ω_k, centered in $\mathbf{x}_k$, as the set of $\mathbf{x} \in \Omega$ s.t.

$$\|\mathbf{x} - \mathbf{x}_k\|_{T_k} < \rho_k,$$

where ρ_k is chosen so that the union of the sets Ω_k, $k = 1, \dots, N$ represents a covering of Ω. Then we define the kth compactly supported nodal *anisotropic weight function* as

$$\bar{W}_{T_k}(\mathbf{x}) = \frac{W_{T_k}(\mathbf{x})}{\sum\limits_{i=1}^N W_{T_i}(\mathbf{x})}, \qquad \text{with } W_{T_k}(\mathbf{x}) = \left[\frac{(\rho_k - D_{T_k}(\mathbf{x}))_+}{\rho_k D_{T_k}(\mathbf{x})}\right]^{\gamma_k}, \tag{11}$$

where $D_{T_k}(\mathbf{x}) = \|\mathbf{x} - \mathbf{x}_k\|_{T_k}$ and γ_k is a positive number, which determines the regularity of the kth weight function. Finally, the *locally anisotropic interpolant* is given by

$$F_A(\mathbf{x}) = \sum_{k=1}^N \bar{W}_{T_k}(\mathbf{x}) R_{T_k}(\mathbf{x}) = \sum_{k \in N_\mathbf{x}} \bar{W}_{T_k}(\mathbf{x}) R_{T_k}(\mathbf{x}), \tag{12}$$

where $N_\mathbf{x}$ is the set of indexes of all the nodes $\mathbf{x}_k$ s.t. $\|\mathbf{x} - \mathbf{x}_k\|_{T_k} < \rho_k$, namely, the nodes whose influence region Ω_k contains $\mathbf{x}$.

In order to characterize (12) as the expected locally anisotropic interpolant, we require the anisotropic weight functions (11) to satisfy certain properties analogously to the Euclidean case. The following theorem establishes that they satisfy the cardinality and partition of unity properties, as their Euclidean analogs, and like the latter have continuous partial derivatives which vanish at the interpolation nodes.

THEOREM 3. *The anisotropic weight functions $\bar{W}_{T_k}(\mathbf{x})$ defined in (11) satisfy the following properties:*

1. $$\bar{W}_{T_k}(\mathbf{x}) \geq 0, \qquad \text{for } \mathbf{x} \in \Omega \quad \text{and} \quad \operatorname{supp}\left(\bar{W}_{T_k}\right) \equiv \Omega_k, \tag{13}$$

2. $$\bar{W}_{T_k}(\mathbf{x}_i) = \delta_{ik}, \qquad i, k = 1, \ldots, N, \tag{14}$$

3. $$\sum_{k \in N_{\mathbf{x}}} \bar{W}_{T_k}(\mathbf{x}) = 1, \qquad \text{for } \mathbf{x} \in \Omega, \tag{15}$$

4. $$\lim_{\mathbf{x} \to \mathbf{x}_j} \nabla \bar{W}_{T_k}(\mathbf{x}) = \mathbf{0}, \qquad \text{for each } \mathbf{x}_j \in X, \quad \text{if } \gamma_k > 1. \tag{16}$$

PROOF. Property 1 follows immediately from definition (11). By defining

$$B_{T_k}(\mathbf{x}) = [\rho_k - D_{T_k}(\mathbf{x})]^{\gamma_k} \prod_{i \in N_{\mathbf{x}}, \, i \neq k} [\rho_i D_{T_i}(\mathbf{x})]^{\gamma_i}, \tag{17}$$

we have

$$\bar{W}_{T_k}(\mathbf{x}) = \begin{cases} 0, & \text{if } k \notin N_{\mathbf{x}}, \quad \mathbf{x} \in \Omega, \\ \dfrac{B_{T_k}(\mathbf{x})}{\sum\limits_{j \in N_{\mathbf{x}}} B_{T_j}(\mathbf{x})}, & \text{if } k \in N_{\mathbf{x}}, \quad \mathbf{x} \in \Omega. \end{cases} \tag{18}$$

Now, Properties 2 and 3 follow immediately, noting that

$$B_{T_k}(\mathbf{x}_j) = 0, \qquad \text{if } j \neq k. \tag{19}$$

To prove Property 4 we show that for $\gamma_k > 1$

$$\lim_{\mathbf{x} \to \mathbf{x}_k} \nabla [D_{T_k}(\mathbf{x})]^{\gamma_k} = \mathbf{0}, \qquad \text{if } k \in N_{\mathbf{x}}; \tag{20}$$

$$\lim_{\mathbf{x} \to \mathbf{x}_j} \nabla B_{T_k}(\mathbf{x}) = \mathbf{0}, \qquad \text{if } j \in N_{\mathbf{x}}, \quad j \neq k. \tag{21}$$

In fact,

$$\begin{aligned} \nabla [D_{T_k}(\mathbf{x})]^{\gamma_k} &= \nabla \|\mathbf{x} - \mathbf{x}_k\|_{T_k}^{\gamma_k} \\ &= \gamma_k \|\mathbf{x} - \mathbf{x}_k\|_{T_k}^{\gamma_k - 2} T_k (\mathbf{x} - \mathbf{x}_k), \end{aligned}$$

and, when $\gamma_k > 1$, we get (20).

To prove (21), we consider

$$\begin{aligned} \nabla B_{T_k}(\mathbf{x}) = {}&\nabla [\rho_k - D_{T_k}(\mathbf{x})]^{\gamma_k} \prod_{i \in N_{\mathbf{x}}, \, i \neq k} [\rho_i D_{T_i}(\mathbf{x})]^{\gamma_i} \\ &+ [\rho_k - D_{T_k}(\mathbf{x})]^{\gamma_k} \sum_{i \in N_{\mathbf{x}}, \, i \neq k} \left[\rho_i^{\gamma_i} \nabla [D_{T_i}(\mathbf{x})]^{\gamma_i} \prod_{\ell \in N_{\mathbf{x}}, \, \ell \neq i, \, \ell \neq k} [\rho_\ell D_{T_\ell}(\mathbf{x})]^{\gamma_\ell} \right], \end{aligned}$$

and we use (20) to obtain the result.

Property 4 now follows immediately using (20) and (21) in the expression of the gradient of $\bar{W}_{T_k}(\mathbf{x})$. ∎

The properties of the locally anisotropic interpolant $F_A(\mathbf{x})$ can now be easily derived.

- The data interpolation property follows from the interpolation nature of the nodal functions, and from the weight functions property (14).

- The shape reconstruction property follows from (14) and (16), which guarantee the interpolation of the first partial derivatives of the nodal functions at the data points. In fact,

$$\nabla F_A(\mathbf{x}_i) = \sum_{k \in N_\mathbf{x}} \left[\nabla \bar{W}_{T_k}(\mathbf{x}_i) R_{T_k}(\mathbf{x}_i) + \bar{W}_{T_k}(\mathbf{x}_i) \nabla R_{T_k}(\mathbf{x}_i) \right] = \nabla R_{T_k}(\mathbf{x}_i), \qquad i = 1, \dots, N.$$

- For each $\mathbf{x} \in \Omega$, the approximation error of the anisotropic reconstruction $E_{F_A}(\mathbf{x})$ can be bounded, in terms of the approximation errors of the nodal functions [10]. More precisely, denoting by $e_{R_{T_k}}(\mathbf{x})$ the error of the nodal function R_{T_k}, we have

$$E_{F_A}(\mathbf{x}) = \sum_{k \in N_\mathbf{x}} \bar{W}_{T_k}(\mathbf{x}) e_{R_{T_k}}(\mathbf{x}),$$

and using property (15) we get

$$\min_{k \in N_\mathbf{x}} e_{R_{T_k}}(\mathbf{x}) \leq E_{F_A}(\mathbf{x}) \leq \max_{k \in N_\mathbf{x}} e_{R_{T_k}}(\mathbf{x}).$$

- The regularity of $F_A(\mathbf{x})$ depends on the regularity of the nodal and weight functions that contribute to the reconstruction in $\mathbf{x}$. In fact, if, for $k = 1, \dots, N$, $R_{T_k} \in C^{\ell_k}(\Omega)$ and we set $\gamma = \min_{k \in N_\mathbf{x}} \{\gamma_k\}$ and $\ell = \min_{k \in N_\mathbf{x}} \{\ell_k\}$, we have that $F_A(\mathbf{x}) \in C^s(\Omega)$, where $s = \min\{\gamma, \ell\}$.

Moreover this locally anisotropic interpolant owns intrinsic shape-preserving capabilities, since the locality of the approach allows us to adapt the reconstruction to the different data features. This can be realized by acting on the free parameters at our disposal:

- by choosing a suitable metric for each local interpolant; this makes it possible to adjust the shape of the RBF and the support of the weight functions, in order to single out the most significant data to reproduce the shape characteristics;
- by acting on the smoothness of the interpolant, both changing the regularity of the RBF in the nodal functions and choosing different parameters γ_k in the weight functions; this yields the shape-preserving reconstruction of smooth and sharp features of the data;
- by using, for each local interpolant, RBFs chosen according to the data behaviour and, if possible, by selecting different shape parameters in the RBF; this is the case for inverse multiquadric or multiorder radial basis functions, which can be scaled acting on their free parameters.

4. 3D SHAPE PRESERVING SURFACE RECONSTRUCTION

In this section, we restrict ourselves to the 3D case, and we consider the problem of shape-preserving reconstruction of an unknown object surface, given a cloud of points describing this surface.

A shape-preserving reconstruction typically maintains important object features, such as edges, corners, and flat regions. The extraction of these features from an unorganized cloud of points requires a preprocessing step, which allows us to introduce information on the intrinsic object structures in the reconstruction process. For this reason, in Section 4.1 we propose a preprocessing procedure, based on a local use of principal component analysis of the covariance matrix, which can be used to identify and classify object features [12]. Then we introduce this shape information by modifying the RBF parameters in the reconstruction method proposed in the previous section. Finally, we further use the covariance matrix to determine a suitable metric, which allows us to construct anisotropic radial basis functions, whose anisotropy reflects the local anisotropy of the data.

4.1. Local Surface Classification

Let the set of distinct points $X_0 = \{\mathbf{x}_i\}_{i=1}^{N_0} \subset \Omega \subset \mathbb{R}^3$ be given, whose elements lie on an unknown surface. In this section, we describe a method that makes use of principal component analysis to determine whether a point $\mathbf{x}_k \in X_0$ is part of a planar region, part of an edge, or occurs at a corner.

Given a set of ng points of X_0 near to $\mathbf{x}_k$, denoted by $\text{Neigh}(\mathbf{x}_k) = \{\mathbf{x}_{k_j}\}_{j=1}^{ng}$, the covariance matrix $\mathcal{C}$ of this set of points is

$$\mathcal{C}(\mathbf{x}_k) = \frac{1}{ng} Q Q^\top, \tag{22}$$

where Q is the $3 \times ng$ matrix

$$Q = (\; \mathbf{x}_{k_1} - \bar{\mathbf{x}}_k \quad \mathbf{x}_{k_2} - \bar{\mathbf{x}}_k \quad \cdots \quad \mathbf{x}_{k_{ng}} - \bar{\mathbf{x}}_k \;)$$

and

$$\bar{\mathbf{x}}_k = \frac{1}{ng} \sum_{j=1}^{ng} \mathbf{x}_{k_j}$$

is the centroid of $\text{Neigh}(\mathbf{x}_k)$. The 3×3 matrix $\mathcal{C}(\mathbf{x}_k)$ is symmetric and, in general, positive semidefinite. This matrix can be factored as $V_k \Lambda_k V_k^\top$, where Λ_k is diagonal and V_k is an orthonormal matrix. The diagonal elements of Λ_k are the eigenvalues $\lambda_k^1 \geq \lambda_k^2 \geq \lambda_k^3$ of $\mathcal{C}(\mathbf{x}_k)$ associated with unit eigenvectors $\mathbf{v}_k^1, \mathbf{v}_k^2, \mathbf{v}_k^3$, respectively, which are the columns of V_k. These mutually perpendicular eigenvectors define the three axis directions of a local coordinate frame with origin $\bar{\mathbf{x}}_k$. We use the values of $\lambda_k^1, \lambda_k^2, \lambda_k^3$ to characterize the point $\mathbf{x}_k$. The local neighborhood in which we estimate $\mathcal{C}(\mathbf{x}_k)$ can be classified in four possible cases:

- flat: one eigenvalue, λ_k^3, is very small or equal to zero, and the other two eigenvalues λ_k^1, λ_k^2 have similar finite values, but significantly greater than λ_k^3; the points $\text{Neigh}(\mathbf{x}_k)$ are almost coplanar, and the two eigenvectors associated with λ_k^1, λ_k^2 form the plane that fits the points; $\mathbf{x}_k$ belongs to a flat region;

- edge: two eigenvalues λ_k^2, λ_k^3 are very small or equal to zero, and λ_k^1 has a finite greater value. The corresponding eigenvector $\mathbf{v}_k^1$ identifies the direction along which the points $\text{Neigh}(\mathbf{x}_k)$ are distributed; $\mathbf{x}_k$ is close to, or on, an edge and $\mathbf{v}_k^1$ is the orientation of the edge;
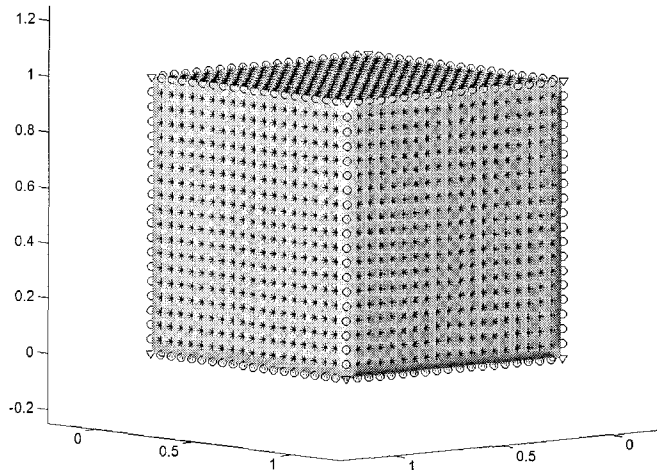

Figure 2. Different markers representing the features detected on a cube data set ($N_0 = 2168$, $ng = 7$); ($*$) flat points, ($\circ$) edge points, and ($\triangledown$) corner points.

- corner: all three eigenvalues have finite, nearly equal values; the point set within $\mathrm{Neigh}(\mathbf{x}_k)$ is likely to be a corner;
- null: no local structure is detected locally.

As an example we show, in Figure 2, the result of our local surface classification method for a cube data set. The different markers represent the different classification of the points.

It is worthwhile noting that the above classification is surely effective for objects with well-defined geometry, while it can present some ambiguities for real or noisy data. In fact, in the latter case, it is difficult to decide if an eigenvalue is really dominant, or if it is small. It is therefore necessary to choose some thresholds which are determinant for the classification, yielding, in this way, threshold dependent features. This is not the case if the object geometry is well identifiable. Another problem can be represented by the data density. In fact, the principal component analysis requires a sufficient sampling density when two components of a surface are separated by a relatively small distance. In this case, the method can fail; that is, it can incorrectly consider in $\mathrm{Neigh}(\mathbf{x})$ points from both components of the surface.

4.2. 3D Locally Scaled Reconstruction

The first approach we consider for a shape-preserving reconstruction consists of the introduction of the previously identified shape information in the isotropic version of the reconstruction method, presented in Section 3. This can be realised by considering the RBFs that depend on some parameters, and by locally modifying these free parameters to appropriately model the local nature of the surface, while leaving the basis functions radially symmetric. For example, using the inverse multiquadric RBF
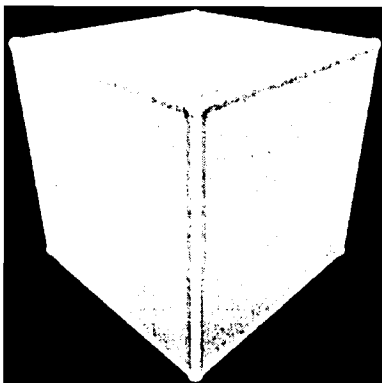
$$\varphi(r) = \left(r^2 + c^2\right)^{-1/2}$$

we can use the free parameter c as a shape parameter. Specifying c to be relatively small for corner and edge points, but increasing it at planar points, we get a suitable scaling of the basis functions to obtain a smooth reconstruction, while preserving sharp features. Using multiple order RBF defined in [13] as
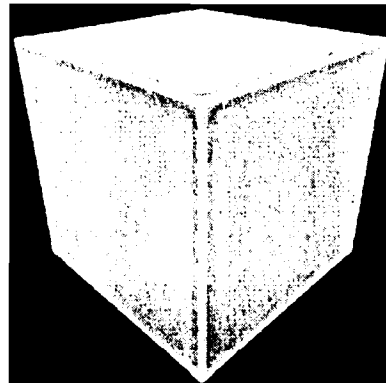
$$\varphi(r) = \frac{1}{4\pi\delta^2 r}\left[1 + \frac{1}{v-w}\left(we^{-\sqrt{v}r} - ve^{-\sqrt{w}r}\right)\right],$$

where

$$v = \frac{1 + \sqrt{1 - 4\tau^2\delta^2}}{2\tau^2}, \qquad w = \frac{1 - \sqrt{1 - 4\tau^2\delta^2}}{2\tau^2},$$

(a) Constant shape parameter.   (b) Feature adapted shape parameter.

Figure 3. Reconstructions of the cube data set using isotropic inverse multiquadric RBFs.

we can influence the free parameters δ and τ by associating increased values for δ and small values for τ at corner and edge points, while reducing δ and increasing τ values at planar points, to let the basis function fall off less rapidly toward zero, and to make its center become increasingly smooth.

For compactly supported RBF, we can reduce the support at corner and edge points, while enlarging it in the flat regions.

The effect of the local scaling of the inverse multiquadric RBFs is shown in Figure 3, where the reconstruction of the cube data set by means of the interpolant (12) with $T = I$ (identity matrix) is presented. As a comparison, we also display the reconstruction obtained using the same parameter for all local interpolants. It is clear that the local reduction of the shape parameter in correspondence with the edges and corners yields an implicit function, whose level set better captures the sharp features of the object.

4.3. 3D Locally Anisotropic Reconstruction

We now consider a shape-preserving reconstruction of an object surface based on the locally anisotropic interpolant (12). The key point is to choose, for each local interpolant, a suitable metric to allow us to model the local data anisotropy. To this aim, we make use of the covariance matrix defined in (22), evaluated, for each $\mathbf{x}_k \in X$, by considering the ng points of X_0 nearest to $\mathbf{x}_k$ that guarantee the nonsingularity of $\mathcal{C}(\mathbf{x}_k)$. This symmetric positive definite matrix defines a set of ellipsoids, centered in $\bar{\mathbf{x}}_k$, and whose semiaxis, oriented as the eigenvectors, are of lengths proportional to the inverse of the corresponding eigenvalues. In order to capture the anisotropy of the data, we need anisotropic radial basis functions, whose anisotropy is the same as the data, namely, whose level sets are ellipsoids with semiaxis lengths *directly* proportional to the eigenvalues. Therefore, we choose the matrix T_k, defining the local anisotropy of the interpolant $R_{T_k}(\mathbf{x})$, as being proportional to the inverse of the covariance matrix, i.e.,

$$T_k = s_k \mathcal{C}^{-1}(\mathbf{x}_k) = s_k V_k \Lambda_k^{-1} V_k^\top \tag{23}$$

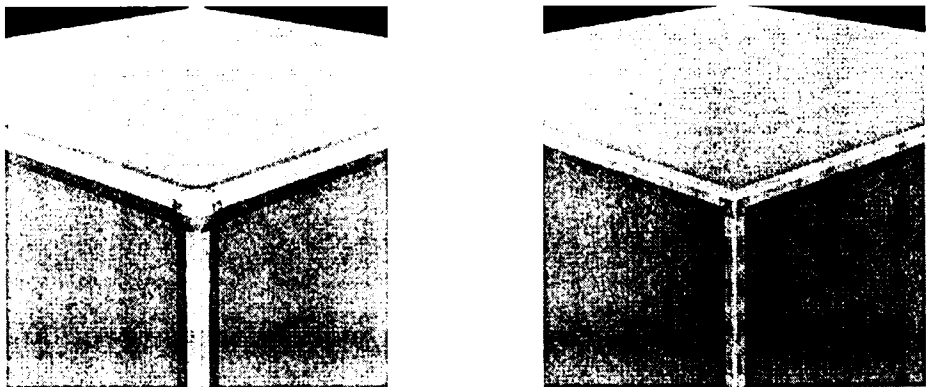with $s_k > 0$. As a consequence, the transformation matrix M_k is given by

$$M_k = s_k^{1/2} \Lambda_k^{-1/2} V_k^\top .$$
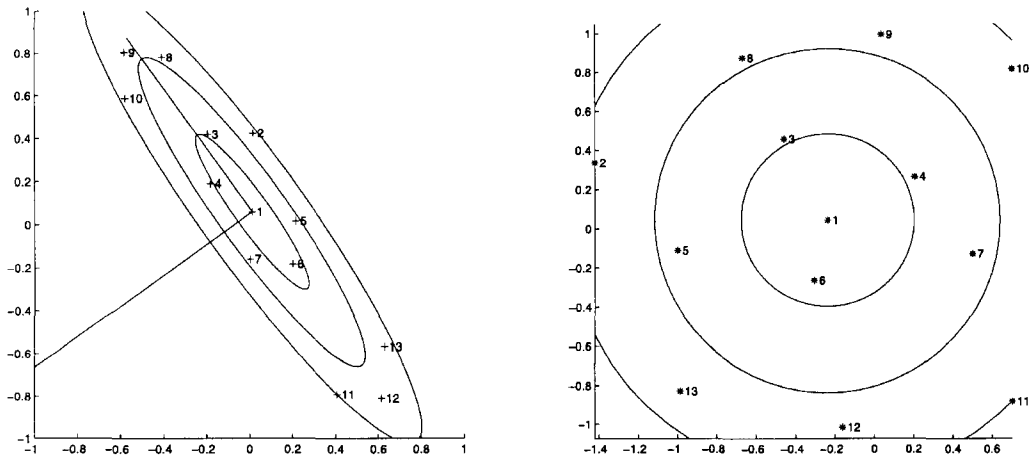
(a) Set X_k and level sets of an anisotropic RBF.

(b) Transformed set Y_k and level sets of the corresponding isotropic RBF.

Figure 4.

(a) Isotropic inverse multiquadric RBFs with   (b) Anisotropic RBFs with feature-adapted
constant shape parameter.   shape parameters.

Figure 5. Zoom of reconstructions of the cube data set.

The normalization constant s_k can be used to improve the stability and accuracy of the anisotropic RBF local interpolant by suitably scaling the eigenvalues of the matrix T_k. In fact, as stated in Theorem 2, the separation and fill distances of the transformed set Y_k strictly depend on these eigenvalues.

To demonstrate the effectiveness of our choice in capturing the data anisotropy, in Figure 4 we show, for the 2D case, the level sets of an anisotropic RBF, deformed according to the data-dependent matrix $T = s\mathcal{C}^{-1}(\mathbf{x}_1)$. The corresponding set $Y = \{\mathbf{y}_i; \ \mathbf{y}_i = M\mathbf{x}_i, \ \mathbf{x}_i \in X\}$, where $M = s^{1/2}\Lambda^{-1/2}V^\top$, and $s = (1/2)\lambda_{\max_{\mathcal{C}(\mathbf{x}_1)}}$ is also shown.

To illustrate the behavior of our method, a prototype algorithm has been implemented and tested both on synthetic data sets and on data from scanned objects. The visualization phase of the resulting surface is based on a marching cube algorithm, which uses the evaluation of the interpolant $F_A(\mathbf{x})$ on points of a uniform grid on the domain Ω, containing the data points.

To better appreciate the quality of the shape-preserving reconstruction provided by the method, we used a cube data set ($N_0 = 2168$ and $N_1 = 820$), where all the shape features are clearly present. The image in Figure 5b shows a detail of the reconstructed surface, obtained using anisotropic inverse multiquadric RBFs with feature-adapted shape parameters. For comparison, Figure 5a shows the reconstruction obtained using isotropic inverse multiquadric RBFs and constant shape parameters. The differences between the two reconstructions are more evident at the edges and corners, since the introduction of the anisotropy of the data, both in the RBFs and in the weight functions, allows the reconstruction to present a sharper and better-defined geometric behavior.

To show the performance of our algorithm on real scanned data sets, we present here the reconstruction of a 20 cm tall model of the Statue of Liberty from an unorganized cloud of points, which consists of $N_0 = 78563$ surface points and $N_1 = 40312$ off surface points.

The reconstruction of the Statue of Liberty realized using anisotropic multiquadric RBFs with feature-adapted shape parameters is shown in Figure 6. From the front and back views of the reconstruction we can appreciate the algorithm's ability to reproduce the features of the model. The detail of the crowned head, evaluated on a finer grid, is shown in Figure 7b, where we also show, as a comparison, the isotropic reconstruction with constant shape parameters (see Figure 7a). Again it is clear that the use of the shape and data anisotropy information yields a reconstruction that better captures sharp features, while smoothing out the flat regions of the crown.

Finally, we would like to note that the visualization of the reconstructed surface is strongly influenced by the method used for extracting the zero level set from the computed implicit
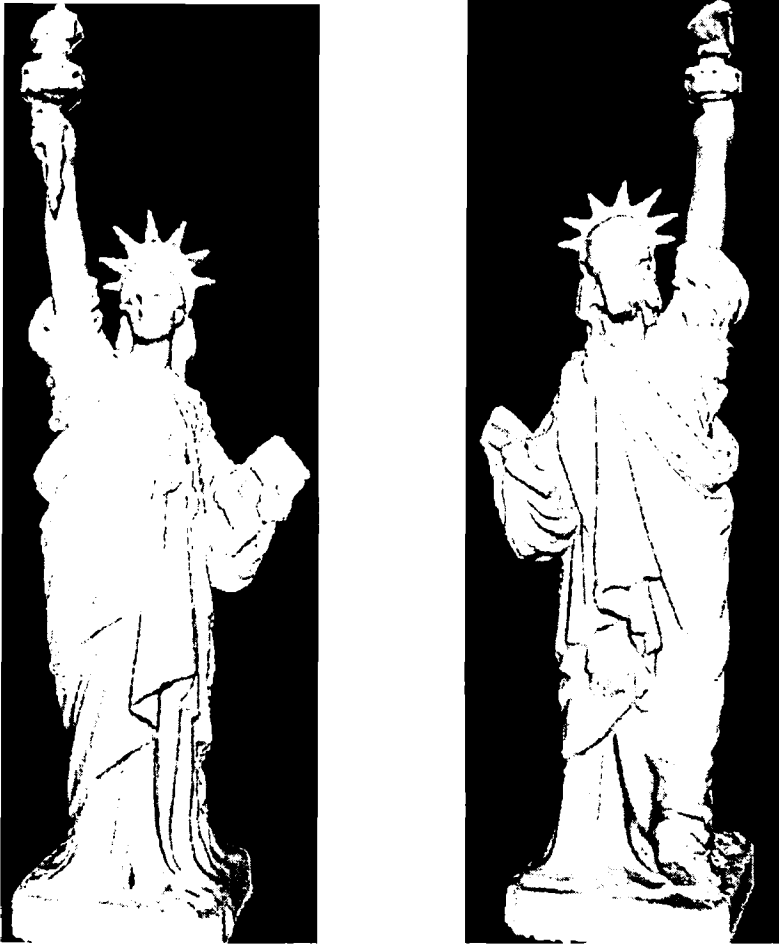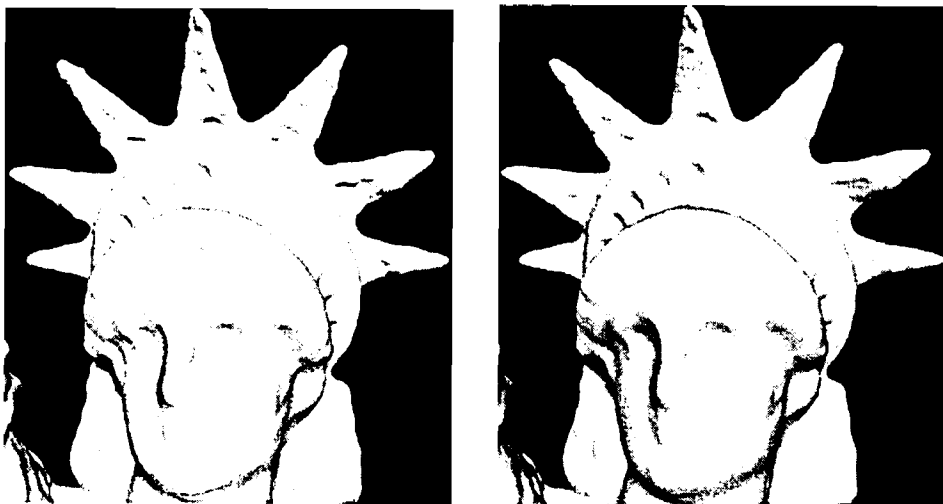
Figure 6. Reconstructions of the Statue of Liberty data set ($N_0 = 78563$, $ng = 30$) using anisotropic inverse multiquadric RBFs with feature-adapted shape parameter.

(a) Isotropic inverse multiquadric RBFs with constant shape parameter.

(b) Anisotropic RBFs with feature-adapted shape parameters.

Figure 7. Detail of the reconstructions of the Statue of Liberty data set.

function. Using, for example, polygonalization of an isosurface of an implicit function can produce apparent faceting (space aliasing) which is a common problem arising from the discretization of a continuous domain. Such a faceting effect is more evident for a shape with sharp features. Since in this paper we focused on a reconstruction algorithm, we have not taken care of the visualization problem and we have simply used the most common marching cube algorithm for extracting the zero level set. Obviously, ray tracing and any more sophisticated polygonalization algorithm could be used in order to produce better quality images. For example, an adaptive resolution algorithm can be considered in which the discrete sampling rate adapts to the changing feature size of the isosurface being polygonized. A good review of adaptive methods can be found in [14].

REFERENCES

1. D. Lazzaro and L.B. Montefusco, Radial basis functions for the multivariate interpolation of large scattered data sets, *Journal of Computational and Applied Mathematics* **140**, 521–536, (2002).
2. G. Turk, H.Q. Dinh, J.F. O'Brien and G. Yngve, Implicit surfaces that interpolate, In *Proc. of Shape Modeling International*, Genoa, Italy, pp. 7–11, (2001).
3. G. Turk and J.F. O'Brien, Modelling with implicit surfaces that interpolate, *ACM Transaction on Graphics* **21** (4), 855–873, (2002).
4. J.C. Carr, R.K. Beatson, J.B. Cherrie, T.J. Mitchell, W.R. Fright, B.C. McCallum and T.R. Evans, Reconstruction and representation of 3D objects with radial basis functions, In *Proc. of SIGGRAPH 2001*, pp. 67–76, ACM Press, (2001).
5. J.C. Carr, R.K. Beatson, B.C. McCallum, W.R. Fright, T.J. McLennan and T.J. Mitchell, Smooth surface reconstruction from noisy range data, In *Proc. of Graphite 2003*, pp. 119–126, ACM Press, (2003).
6. M. Bozzini, L. Lenarduzzi, M. Rossini and R. Schaback, Interpolation by basis functions of different scales and shapes, *Calcolo* **41**, 77–87, (2004).
7. G. Casciola, D. Lazzaro, L.B. Montefusco and S. Morigi, Fast surface reconstruction and hole filling using radial basis functions, *Numerical Algorithms* **39**, 289–305, (2005).
8. G.M. Nielson, Coordinate free scattered data interpolation, In *Topics in Multivariate Approximation*, (Edited by L.L. Schumaker *et al.*), pp. 175–184, Academic Press, New York, (1987).
9. R. Schaback, Lower bounds for norms of inverses of interpolation matrices for radial basis functions, *Journal of Approx. Theory* **79**, 287–306, (1994).
10. R. Schaback, Error estimates and condition numbers for radial basis function interpolation, *Adv. Comput. Math.* **3**, 251–264, (1995).
11. R. Schaback, Stability of radial basis function interpolants, In *Approximation Theory X: Wavelets, Splines, and Applications*, (Edited by C.K. Chui *et al.*), pp. 433–440, Vanderbilt Univ. Press, Nashville, TN, (2002).
12. H. Hoppe, T. De Rose, T. Duchamp, J. McDonald and W. Stuetzle, Surface reconstruction from unorganized points, In *Proceedings of ACM SIGGRAPH*, pp. 71–78, (1992).
13. F. Chen and D. Suter, Multiple order Laplacian splines—Including splines with tension, Technical Report Department of Electrical and Computer Systems Engineering, Monash University, Clayton, Australia, (1996).
14. J. Bloomenthal, *Introduction to Implicit Surfaces*, Morgan Kaufmann, San Francisco, CA, (1997).